Alexandria Engineering Journal (2020) 59, 1515–1524

HOSTED BY

Alexandria University

Alexandria Engineering Journal

www.elsevier.com/locate/aej
www.sciencedirect.com

Hydrodynamic self-excited vibrations in leaking spherical valves with annular seal

Hesham Awad [a], Jorge Parrondo [b]

[a] Arab Academy for Science, Technology & Maritime (AASTMT), Mechanical Engineering Department Alexandria, Egypt
[b] Universidad de Oviedo, Departmento de Energía, Gijón, Spain

Received 28 November 2019; revised 4 February 2020; accepted 27 March 2020
Available online 6 June 2020

KEYWORDS

Flow induced vibration;
Self-excited vibrations;
Salime hydroelectric power plant;
Periodic leakage flow;
Pressure fluctuation generation;
Perturbation technique

Abstract Occasionally, annular seals of ball valves in hydro power plants may not perform their sealing function adequately but develop periodic vibration with periodic leakage rates causing high amplitude pressure fluctuations in the penstocks. The aim of the present study is to develop a simplified model that can explain the excitation mechanism and estimate the behavior of the hydro-mechanical system depending on the geometrical and physical parameters. The stability of the system has been studied in order to yield recommendations for best operating conditions. The governing equations are nonlinear and the perturbation technique has been adopted to solve the system variables. Following, a dimensionless analysis was developed to gain more knowledge on the parameters affecting this phenomenon. A MATLAB code was designed and implemented to study the system stability for different input reservoir energy levels and different system configurations. The results show that the system stability depends on the relation between the main line inertia and the leakage kinetic energy, the leakage reduced velocity, the seal surface area ratio, the pilot line geometry and the hydraulic losses. Also, solving the hydro-mechanical model nonlinearly brings about oscillation amplitudes that exceed the gap clearance as it is very small and the seal will hit the ball surface going backward and forward.

1. Introduction

Fluid-dynamic systems with flow control valves can develop flow-excited vibrations if the head loss– flow rate curve of the valve under transient conditions has a negative slope, i.e. if the flow rate reduces for increasing head [1,2]. That is not uncommon for plug valves operating at small openings or for leaking valves whose clearance increases for head diminishing. Examples of the latter can be found in the large size spherical valves installed in some high pressure pipelines, including the penstocks of many hydro power plants like the Salime plant in Asturias (Spain) [3]. This is an impoundment plant of 105 m in nominal net head, four units with independent penstock and Francis turbine and a rated power output of 40 MW/unit after a refurbishment of the plant one decade ago. Just upstream of each turbine, a spherical valve is to be closed when the unit is not in operation to stop water flowing from the reservoir (Fig. 1a).

E-mail addresses: hesham.saber@aast.edu (H. Awad), parrondo@uniovi.es (J. Parrondo)

Peer review under responsibility of Faculty of Engineering, Alexandria University.

https://doi.org/10.1016/j.aej.2020.03.033

Nomenclature

ϕ	seal diameter [m]	H_i	total energy head at section *i* [m]
A_i	cross section area at section *i* [m^2]	I	area moment of inertia [m^4]
A_{SS}	seal surface area facing gap flow [m^2]	I_i	water inertia coefficient through a specific pipeline i [s^2 m^{-2}]
A_{OS}	annular seal external area facing pilot pipe line [m^2]	K_S	annular seal stiffness [N m^{-1}]
C_{sg}	annular seal damping coefficient corresponding to gap angle [N s m^{-1}]	K_i	total friction loss coefficient at section *i*
d_i	diameter at section *i* [m]	K_{Li}	minor friction loss coefficient at section *i*
E	modulus of elasticity [Pa]	M_S	annular seal mass [kg]
f_i	friction factor at section *i*	P_i	total pressure at section *i* [Pa]
g	gravitational acceleration [m s^{-2}]	Q_i	total flow rate at section *i* [l s^{-1}]
		t	time [s]

In order to prevent leakage between sphere and casing when the valve is closed, that annular passage can be blocked by sliding a retractable ring seal onto the ball surface (Fig. 1b). In the case of the Salime plant, the driving force to shift the seal to closure position is obtained by applying high pressure water on its external surface, by means of a duct coming from the penstock (Fig. 1c). In practice, however, it was noticed on different occasions that, with a unit in standby mode and the spherical valve closed, the seal did not really stay fixed on the ball but developed periodic vibrations, which were perceived as a succession of violent internal impacts at a rate of 1–3 Hz accompanied by high pressure fluctuations in the hydraulic system. The phenomenon ended when an alarm sensor at the valve inlet detected pressure values above a security limit established in 13.5 MPa, which triggered the closure of a double butterfly valve at the penstock intake thus preventing any leakage. The instruments available in the plant were not intended to register signals at a sufficiently low time step, and so no adequate pressure or acceleration signals could be obtained during those episodes. Even so, the rate of fluctuations was estimated to lie in the range 1–3 Hz, with different values depending on the unit and on the available gross head. This suggested that the vibrations would be associated to the existence of a gap between seal and ball when the static fixing forces on the seal were not high enough. Hence, an auxiliary compressed air system was installed to increase the forces on the seal of each valve during valve closure. The method has proved to be very effective to avoid the excitation, though the phenomenon has still been observed to appear if eventually the compressed air system was not operational.

All this behavior suggests that the vibrations are self-excited and related to unsteady leaking flow through a fluctuating gap between sphere and seal. In fact, this type of problems has been observed in hydro power plants since long

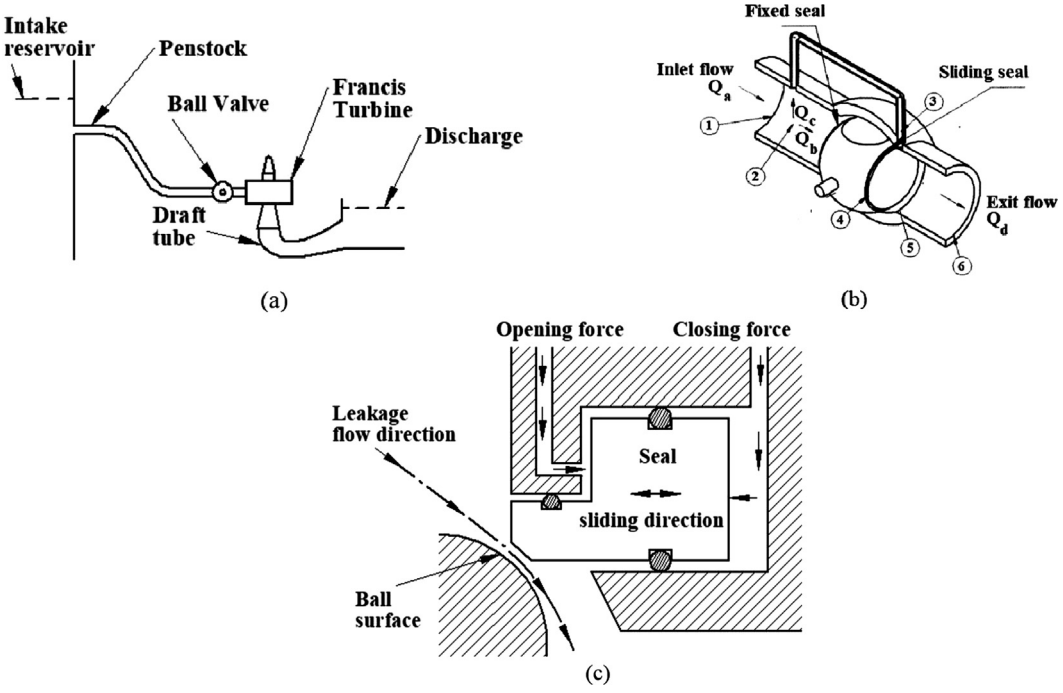

Fig. 1 (a) Salime Hydroelectric Power Plant schematic diagram. (b) Simplified diagram of the closed valve with relevant positions in the seal area and in the pressure (or pilot) application duct on the. (c) Detailed section of the sliding annular seal, applied on its seat.

time ago, though the cases reported in the literature are very scarce. An early and exceptionally well-documented case was reported by Abbot et al. [4] and further analyzed by Wylie and Streeter [5] on the auto-oscillations in the penstock of the Bersimis No. 2 plant (Canada). The origin was attributed to intermittent leakage because of inadequate sealing in a spherical valve, though the service seal was not retractable but flexible and inflatable. Gummer [6] reported on the severe penstock resonances registered in the Maraetai No. 1 hydro station (New Zealand), which were produced after load rejection or during priming. In that case, the origin was located not at a spherical valve but at the head gate seal, which is also inflatable, due to poor oil pressure application. More recently, Kube et al. [7] mentioned a case of penstock pressure pulsations in the Gordon hydro plant (Australia) that were originated by a leaking spherical valve with retractable seal, similar to the case of the study now presented.

The problem of self-excited oscillations in hydro systems with leaking valves can be compared to similar processes in other types of valves and gates that operate at small openings, for which there is a more abundant literature [8,9]. A common feature for the instability to develop is that the fluid system and the obstructing element of the valve, when set into oscillatory motion, couple in such a way that the resulting dynamic forces on the element reinforce its motion, thus allowing for a sustained supply of fluid energy to the structure. Main situations leading to destabilizing forces can be broadly classified in two groups: flow inertia and fluid-acoustic couplings. In the first group of cases, the flow inertia is responsible for a lag in the velocity and pressure fields while adapting to the clearance change as imposed by the motion of the valve element. This category includes cases of self-excitation in spring loaded valves such as swing check valves [10], plug valves [11,12] and poppet valves [13], as well as hydraulic gates [9]. In the mathematical modeling of these systems, the plug or vibrating element is usually represented by 1DOF mass, the inertia effects are mostly contributed by the flow fluctuations in the conduits and the valve passage is modeled as an orifice with variable cross-section and a discharge coefficient that can incorporate hysteresis features [11,12]. Calculation of fluid forces on the vibrating element leads to the analysis of the post-stable behavior of the system and to establishing stability conditions. This can reveal systems being stable or unstable depending on the amplitude (low or high) of an initial perturbation [13], and can lead to the design of specific stability techniques [14].

In the second group of cases, the acoustic response of the system determines the fluid force on the vibrating element, usually a spring-loaded poppet or plate in a pressure relief valve, so that vibrations can take place at an acoustic resonance mode of the piping. The development of instability due to acoustic coupling in valves that would otherwise be stable has been observed in several recent experimental studies with different set-up configurations and working fluids, including both liquids [15,16] and gases [17,18]. Modeling of these systems to obtain the forces on the vibrating element may be done by including fluid compressibility in the equations for unsteady gas flow, like Hos et al [19], or by assuming plane wave propagation along the pipes, as done by Misra et al. [20] for a control valve operated by a pneumatic drive, or using a method of characteristics

With these mentioned studies, the aim of the presented study is to develop a simplified theoretical model that can explain the excitation mechanism for the seal vibrations and estimate the behavior of the hydro-mechanical system, having more depth on understanding the parameters affecting the vibration phenomenon taking into consideration seal characteristics and dynamics, establishing conditions of stable and unstable operation and to give recommendations for best operating conditions.

2. Seal specification

It is assumed that the seal may have an imperfection in manufacture or an assembly imperfection. According to that it is expected that only one portion of the seal will have a clearance leading to leakage as in Fig. 2. The thickness of the clearance will vary through the defected portion of the seal. However, for the present analysis, it is sufficient to consider an average thickness y_{av} as well as mean vibration amplitude for the seal.

2.1. Annular seal characteristics

So as to simulate the annular seal equation of motion, the annular seal characteristics corresponding to the gap length such as annular seal stiffness, mass and damping coefficients must be estimated first.

2.1.1. Annular seal stiffness coefficient

In order to calculate the annular seal stiffness, the annular seal deflection due to the applied load is required. Considering the annular seal as a curved beam such as shown in Fig. 2, Castigliano's theorem could be utilized to estimate the annular seal deflection as for a fixed support-uniform load straight beam configuration [21]. Besides, by integrating the deflection equation and equating it with the average area, the average deflection can be calculated. Afterwards, by replacing the annular seal length by the gap length L_{sg} and dividing the applied load by the average deflection the annular seal stiffness through a certain gap can be calculated by the following equation.

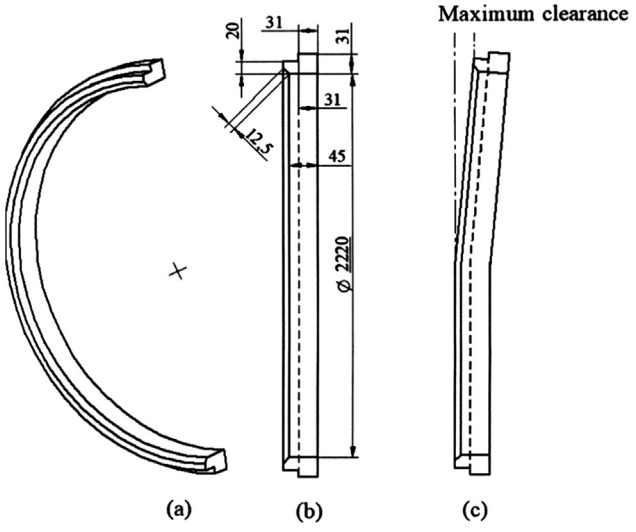

Fig. 2 (a) Annular seal section view. (b) Un-deformed annular seal side view with dimensions in mm. (c) Deformed annular seal side view with maximum clearance position.

$$K_{sg} = \left| -\frac{720\,EI}{L_{sg}^{3}} \right| \tag{1}$$

where $L_{sg} = L_s\left(\frac{\theta_{gap}}{2\pi}\right)$, θ_{gap} is the gap angle and $L_s = \pi\phi$.

2.1.2. Annular seal mass coefficient

The annular seal mass equation corresponding to the gap angle can be calculated as following.

$$M_{sg} = M_s\left(\frac{L_{sg}}{L_s}\right) = M_s\left(\frac{\theta_{gap}}{2\pi}\right) \tag{2}$$

2.1.3. Annular seal damping coefficient

Once the values of the annular seal mass and stiffness corresponding to the gap length are calculated, the damping coefficient can be determined from the damping factor equation as follows,

$$C_{sg} = 2\zeta\sqrt{M_{sg}K_{sg}} \tag{3}$$

3. Theoretical model

The case of interest is related to Movement Induced Excitation, (MIE) flow induced vibration [8], as the fluid dynamic force is supported by the oscillatory motion of the vibrated seal. In order to make the theoretical model as simple as possible and containing all the relevant data of the real plant, it is decided to consider the main and the spherical valve scheme of Fig. 1b.

According to Fig. 1b, in order to obtain the pressure and flow rate at different mechanical system sections, the energy equation for an unsteady, unidirectional, incompressible and viscous flow is utilized across the relevant hydraulic pipes together with the continuity equation across each junction [23] and the seal equation of motion. The mechanical-hydraulic system for each group of the hydroelectric power station under consideration can be summarized in the diagram of Fig. 3.

Point 1 presents the entrance to penstock from input reservoir, point 2 is the pilot pressure take off acting on the annular seal, point 3 is the external face of the annular seal in which the pilot pressure is applied, point 4 resembles the sliding annular seal gap clearance while point 5 is the discharge tube entrance, point 6 is the discharge chamber, L_a is the penstock length up to valve inlet, L_{b1} is the duct length through spherical valve to ball entrance, L_{b2} is the fixed seal length in flow direction, L_{b3} is the Length between fixed seal and sliding seal, L_g is the gap length, L_d is the length from ball exit to discharge, L_c is the pilot pipeline length and, y_{gu} is the unloaded clearance thickness, as the seal is unstrained neither statically nor dynamically, y_{o_g} refers to the average gap thickness after being stressed statically and y is the vibration displacement of the sliding seal from the static equilibrium position. The system governing equations for every section will be presented as follows,

$$\textit{Section } 1-2: \quad H_1 - H_2 = I_a\frac{dQ_a}{dt} + Q_a^2 K_a \tag{4}$$

$$\textit{Section } 2-3: \quad H_2 - H_3 = I_c\frac{dQ_c}{dt} + Q_c K_c \tag{5}$$

$$\textit{Section } 2-4: \quad H_2 - H_4 = I_b\frac{dQ_b}{dt} + Q_b^2 K_b \tag{6}$$

where $K_a = \frac{f_a L_a}{2gd_a A_a^2} + \frac{K_{La}}{2gA_a^2}$, $K_b = \frac{f_{b1}L_{b1}}{2gd_{b1}A_{b1}^2} + \frac{K_{Lb}}{2gA_{b1}^2} + \frac{\left(\frac{1}{A_{b2}} - \frac{1}{A_{b3}}\right)^2}{2g}$, $K_c = \frac{32\,\nu\,L_c}{gA_c d_c^2}$ and $I_i = \frac{L_i}{gA_i}$.

The losses through sections 2–3 are assumed for laminar flow as the velocity of flow in this section is expected to be small. So, the hydraulic loss will be proportional to the flow rate [23] as,

$$Q_g = Q_b + A_{ss}\frac{dy}{dt} \tag{7}$$

Annular seal equation of motion:

$$M_{sg}\ddot{y} + C_{sg}\dot{y} + K_{sg}y = F(t) \tag{8}$$

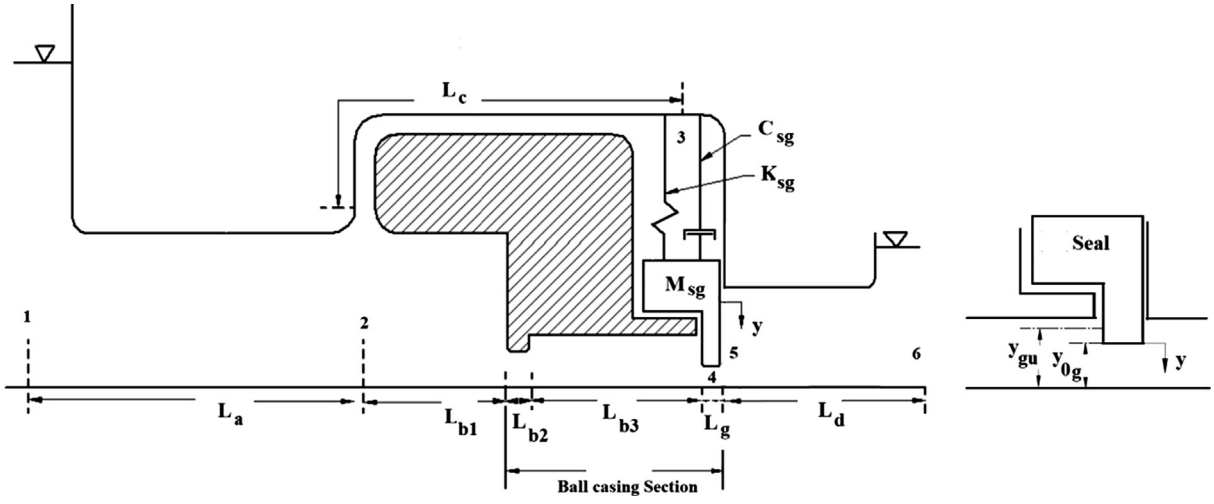

Fig. 3 Simplified mechanical-hydraulic system for each group of the hydroelectric power station with seal clearance geometrical specifications and vibration motion coordinate.

where

$$F(t) = P_3 A_{os} - P_4 A_{ss} \tag{9}$$

$$\textit{Section } 4-5: \quad H_4 - H_5 = \frac{Q_d^2\left(\frac{1}{A_g} - \frac{1}{A_d}\right)^2}{2g} \tag{10}$$

$$\textit{Section } 5-6: \quad H_5 - H_6 = I_d \frac{dQ_d}{dt} + Q_d^2 K_d \tag{11}$$

where $K_d = \frac{f_d L_d}{2g d_d A_d^2} + \frac{K_{Ld}}{2g A_d^2}$.

Gap cross-sectional area:

$$A_g = L_{sg}(y_{og} - y) \tag{12}$$

Energy level at section 1 is a variable while at section 6 is maintained zero.

Pressure at sections 3 and 4:

$$P_3 = \rho g\left(H_3 - \frac{\frac{dy^2}{dt}}{2g}\right) \tag{13}$$

$$P_4 = \rho g H_5 \tag{14}$$

$$\textit{Section } 2-8 \text{ (flow rate)}: \quad Q_c = A_{os}\frac{dy}{dt} \tag{15}$$

3.1. Dynamic system modeling using the perturbation technique

The perturbation technique will be adopted to solve the system variables, as the variables are assumed to be composed of steady state component and time dependent small oscillations components superimposed over them. It can thus be assumed that $Q_i = Q_{oi} + q_i$ and $H_i = H_{oi} + h_i$. Taylor series function will be used to linearize the nonlinear equations.

3.2. Dimensionless analysis:

In order to have a deep understanding of the parameters affecting the problem, a dimensionless analysis is carried out with some simplifications. Firstly, neglecting main line tube hydraulic losses presented at sections 1–2, 2–4 and 5–6 as they have a negligible value compared to the input reservoir energy level and gap leakage kinetic energy. Beside, as the leakage gap cross sectional area is very small compared to the previous cross section A_{b3}, then most of the energy head H_2 is converted to kinetic energy through the gap and the gap pressure head can be assumed as equal to H_5, as the gap kinetic energy will be lost by Bordas loss in section 4–5. After, applying the mentioned simplifications, the analysis showed that the dimensionless added water damping, stiffness and mass mentioned briefly in Appendix A are function of the following pi groups:

$$\left(C_w^*, K_w^*, M_w^*\right) = f\left(\Pi_1, \Pi_2, \Pi_3, I_a^*, I_b^*, I_c^*, I_d^*, \gamma\right) \tag{16}$$

$$\Pi_1 = \frac{\text{Gap kinetic energy}}{\text{Main line Inertia}} = \frac{\frac{v_{og}^2}{2g}}{I_m w_{ref} Q_{og}}, \qquad \Pi_2$$

$$= \text{Gap reduced velocity} = \frac{v_{og}}{L_g w_{ref}}, \qquad \Pi_3$$

$$= \frac{\text{Pilot line head loss}}{\text{Main line inertia}} = \frac{K_c}{I_m w_{ref}},$$

$$I_a^* = \frac{I_a}{I_m}, \quad I_b^* = \frac{I_b}{I_m}, \quad I_c^* = \frac{I_c}{I_m}, \quad I_d^* = \frac{I_d}{I_m} \quad \text{and} \quad \gamma = \frac{A_{ss}}{A_{os}}$$

where $I_m = I_a + I_b + I_d$, $w_{ref} = \sqrt{\frac{K_{sg}}{M_{sg}}}$.

4. Conditions of stability

So, after applying the simplifications and the dimensionless analysis, the seal equation of motion will be as follows,

$$y^*\left(\frac{M_{sg}}{\rho g I_m A_{os}^2} + M_w^*\right) * + \dot{y}^*\left(\frac{C_{sg}}{\rho g I_m A_{os}^2 w_{ref}} + C_w^*\right) + y^*\left(\frac{K_{sg}}{\rho g I_m A_{os}^2 w_{ref}^2} + K_w^*\right) = 0 \tag{17}$$

M_w^*, C_w^* and K_w^* resemble as well the dimensionless fluctuating components of the instantaneous force F(t) in Eq. (9) as a combination of terms proportional to the displacement, velocity and acceleration of the seal vibration [8]. Also, Eq. (17) presents the equation of motion for a single degree of freedom free vibration damped system. For such a system the inherent frequency w of the oscillation is determined through the damped frequency equation and the stability is known from the equivalent damping coefficient value of Eq. (17) [22].

5. Computational procedure

To solve the steady state equations, two iteration mechanisms are utilized to determine the flow rate and the gap cross sectional area. Following, the unsteady equations are solved with the aid of the steady state variables. To estimate the correct value of the frequency w and the force coefficients M_w^*, C_w^* and K_w^*, an iteration mechanism is adopted by inserting an initial value for the frequency, calculating the force coefficients in Eq. (17) and the damped frequency. Solution convergence is achieved as the relative error between the frequency values is smaller than 10^{-6}. A MATLAB code is designed to have the ability for studying the effect of Pi-groups variation while varying input reservoir energy level on the dynamic performance of the system.

6. Results

The dynamic performance of the hydro-mechanical system will be discussed through three parameters Π_m, Π_k and Π_c. Π_m presents a ratio between added water mass M_w and pilot water mass multiplied by square seal external surface area ratio to pilot pipe line cross-section area M_c. Π_k presents a ratio between added water stiffness and seal structure stiffness. While, Π_c presents a ratio between added water damping and seal structure damping. Following, stability design charts functions of Π_1, Π_2, I_c^* and γ are developed and finally the nonlinear system is solved including the neglected hydraulic losses to observe its effect on reaching the limit cycle oscillation.

Fig. 4 shows, that the added water mass is independent of Π_1, Π_2 and system oscillation frequency f. On the other hand, Fig. 4c, presents that the added water mass depends on the seal surface area ratio γ and I_c^*. As, by incrementing I_c^* the added

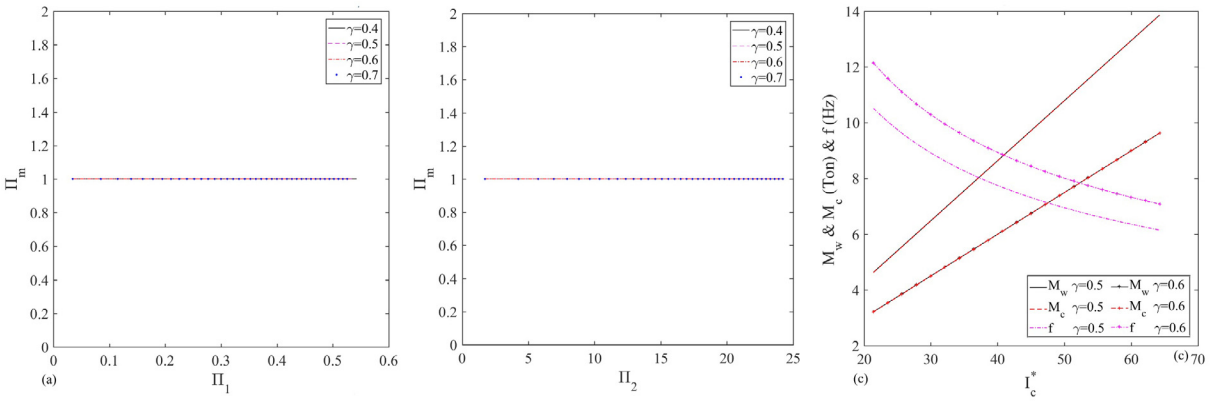

Fig. 4 (a) Relation between Π_m and Π_1. (b) Relation between Π_m and Π_2. (c) Relation between M_w, M_c, f and I_c^* for $\Pi_1 = 0.3634$ and $\Pi_2 = 17.315$. $I_a^* = 0.78$, $I_b^* = 0.03$ and $I_d^* = 0.19$.

water mass M_w and M_c increase while the system oscillatory frequency tends to decrease. On the other hand, incrementing γ tends to reduce M_w and M_c while increasing system oscillation frequency f for the same value of I_c^*.

Basically according to Kolkman (2007) [9] there are three types of added stiffness. This added stiffness could be due to immersion, sudden stiffness as in the case of culvert gates and finally, the added stiffness due to quasi-stationary flow forces which corresponds to the present case. At low values of Π_1, the main pipe line inertia is very high in comparison to gap discharge. That will lead to a pressure build up inside the gap, which tends to lift the seal opposite to the vibration motion, augmenting the seal stiffness. On the other hand, augmenting Π_1 will lead to a pressure reduction inside the gap, which results in a seal suction, increasing the negative stiffness effect such as seen in Fig. 5a.

However, kinetic energy augmentation can be explained as a hydraulic head augmentation that tends to reduce the seal gap area, such as in the case of an orifice or valve with a varying discharge area. At very high hydraulic head the seal gap area reduction is higher in comparison to gap flow velocity augmentation. This relation will lead to a lower augmentation rate or a discharge reduction as shown in Fig. 5c, which in both cases will result in a pressure build up and a lower negative stiffness effects such as mentioned in Fig. 5a. Fig. 5b shows a similar attitude as in Fig. 5a. At very low reduced velocity the seal tends to have a lower negative stiffness due to pressure build up, while augmenting the reduced velocity will lead to a pressure reduction and higher negative water stiffness, but also as mentioned before at very high reduced velocity the discharge flow tends to decrease leading to a lower negative water stiffness. Also, according to the flow rate Eq. (7) increasing the seal surface area facing the gap flow will result in a gap discharge augmentation, gap pressure reduction and lower negative water stiffness response, such as shown in Fig. 5a and b.

Fig. 6a manifests that added water stiffness is independent of Π_3. Also, Fig. 6c shows the independency of the steady state gap flow rate from I_c^* and Π_3. However, the total gap flow rate varies slightly, due to oscillation frequency variation. So, as the total gap flow rate variation from one case to another is small, Π_k variation is a frequency dependent. As seen in Fig. 1c for the case considering Π_1 and I_c^* equals to 0.3634 and 21.43 the equivalent mass coefficient is 4.62×10^3 kg with an oscillation frequency of 10.51 Hz. While, for the same Π_1 but with I_c^* equals to 32.14, the equivalent mass coefficient increased to 6.929×10^3 kg and the oscillation frequency reduced to 8.62 Hz. These results show a mass increment of 33.23% and

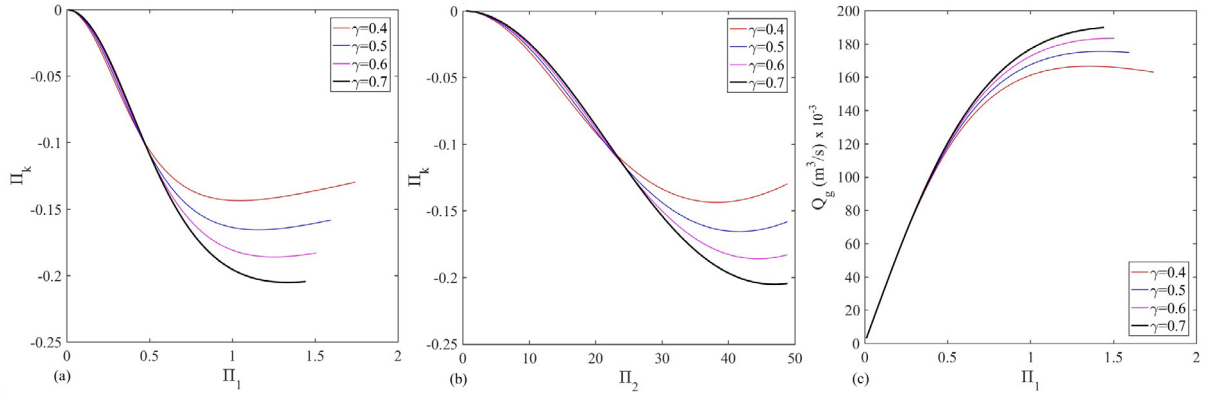

Fig. 5 (a) Relation between Π_k and Π_1. (b) Relation between Π_k and Π_2. (c) Relation between Q_g and Π_1. $I_c^* = 0.78$, $I_b^* = 0.03$, $I_d^* = 0.19$ and $\Pi_3 = 0.0031$.

an oscillation frequency reduction of 17.9%, which results in a higher equivalent stiffness coefficient and a lower negative Π_k values such as seen in Fig. 6b.

Basically the added water damped is mainly caused by the flow velocity. As it can be seen form Fig. 7a and b, as Π_1 and Π_2 increase the flow damping forces tend to excite the system rather than damping it. For the case of $\gamma = 0.4$ as shown in Fig. 7c, for values of Π_1 lower than 0.152 the amplitude of unsteady seal inlet velocity v_1 is higher than the seal outlet velocity v_2 and according to the flow rate Eq. (7) that gives

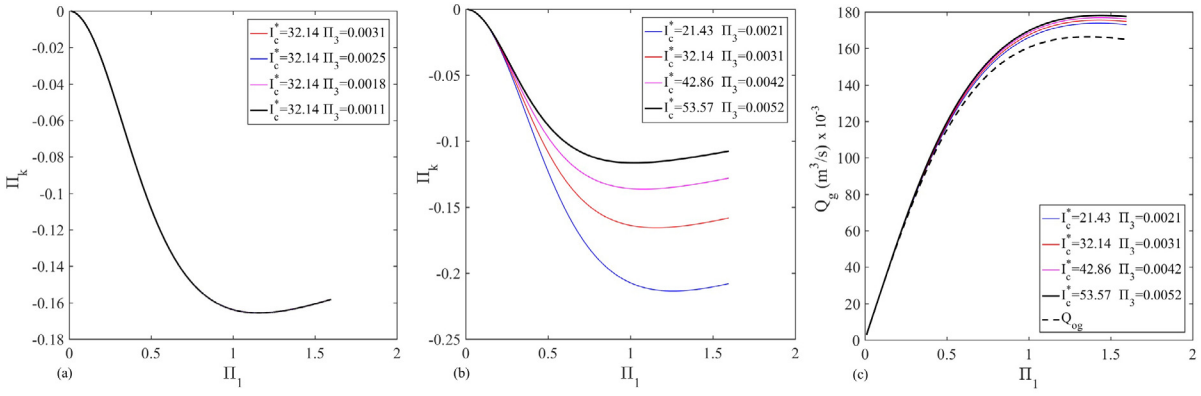

Fig. 6 (a) Relation between Π_k and Π_1. (b) Relation between Π_k and Π_1. (c) Relation between Q_g and Π_1. $I_a^* = 0.78$, $I_b^* = 0.03$, $I_d^* = 0.19$ and $\gamma = 0.5$.

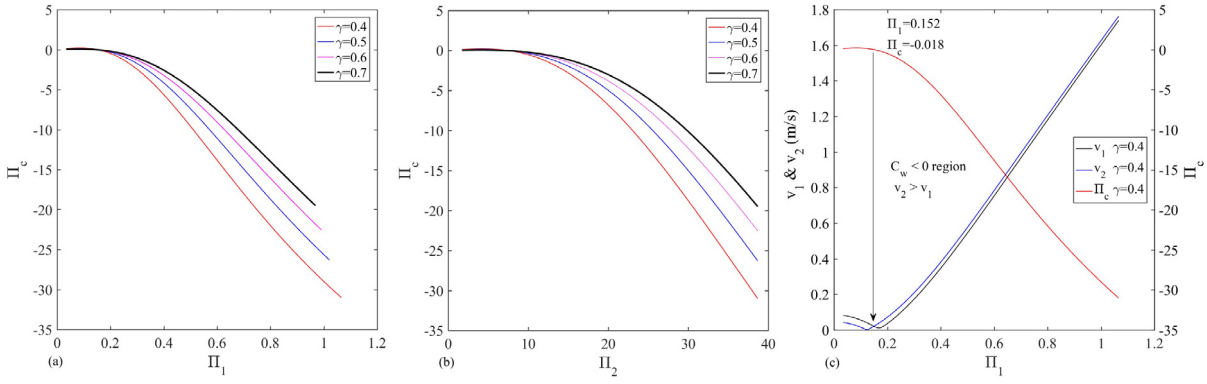

Fig. 7 (a) Relation between Π_c and Π_1. (b) Relation between Π_c and Π_2. (c) Relation between v_1, v_2 and Π_1. $I_a^* = 0.78$, $I_b^* = 0.03$, $I_c^* = 32.14$, $I_d^* = 0.19$ and $\Pi_3 = 0.0031$.

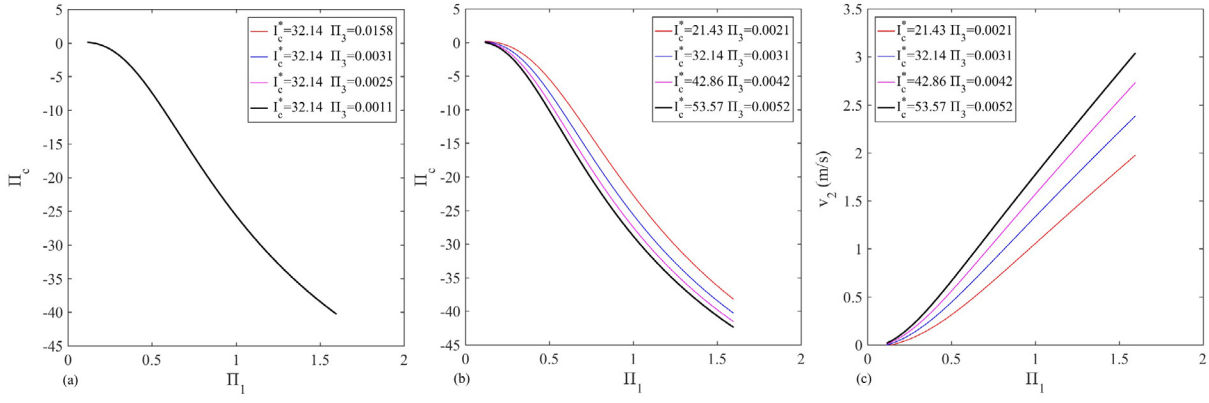

Fig. 8 (a) Relation between Π_c and Π_1. (b) Relation between Π_c and Π_1. (c) Relation between v_2 and Π_1. $I_a^* = 0.78$, $I_b^* = 0.03$, $I_d^* = 0.19$ and $\gamma = 0.5$.

an indication for a flow velocity in the opposite direction of seal vibration, which results in a positive added water damping and seal vibration resistance augmentation. On the other hand, for Π_1 values higher than 0.152, v_2 is higher than v_1, which results in a flow velocity in the seal vibration direction leading to a negative water damping that excites the system rather than damping it. Also, as Π_1 and Π_2 increase the systems tends to be more dynamically unstable for the same value of γ as seen in Fig. 7a and b, as the negative water damping term mentioned in Eq. (A2) is function of Π_1^2 multiplied by Π_2. Seal surface area ratio γ has a significant effect on the water added damping. As, by augmenting γ the total gap flow rate increases as shown in Fig. 5c, however the gap cross section area increases too due to external seal surface area A_{os} reduction. That will lead to v_2 reduction and in turn a lower negative added damping water such as shown in Fig. 7a and b.

Fig. 8a shows a slight effect of Π_3 variation on the added water damping for the same values of I_c^* and γ. Such as, for the highest Π_3 the maximum and minimum Π_c are 0.1577 and −40.2726, while for the minimum Π_3 the highest and lowest values of Π_c are 0.1255 and −40.3052. On the other hand, augmenting I_c^* for a fixed γ increase system instability and exit seal velocity v_2 such as seen in Fig. 8 b and c. As, by varying I_c^* the system oscillation frequency varies, which increases the amplitude of unsteady seal outlet velocity v_2, which results in Π_c reduction.

Fig. 9a shows the stability charts for a varying seal area ratio γ with different seal area configurations for the same I_c^*. Where, for the same γ by incrementing A_{ss} the structure seal damping tends to decrease, so a lower negative water damping, Π_1 and Π_2 are needed to reach the critical dynamic stability condition. Also, as mentioned in Fig. 7a and b incrementing γ leads to a higher dynamic stable system as the positive water damping tends to increase. So, for a higher γ values critical dynamic stability conditions are achieved at higher Π_1 for the same Π_2, as by incrementing Π_1 the gap kinetic energy is increasing with respect to main line inertia leading to more negative water damping. On the other hand, for the same value of Π_1 a lower Π_2 is needed to reach critical dynamic stability conditions for a higher γ. As, by increasing γ the seal structure damping is lowered at a higher rate in comparison to added water damping increment, so a lower Π_2 is needed to reach critical dynamic stability condition. Fig. 9b and c shows the stability design charts for a varying I_c^* and γ as a function of Π_1 and

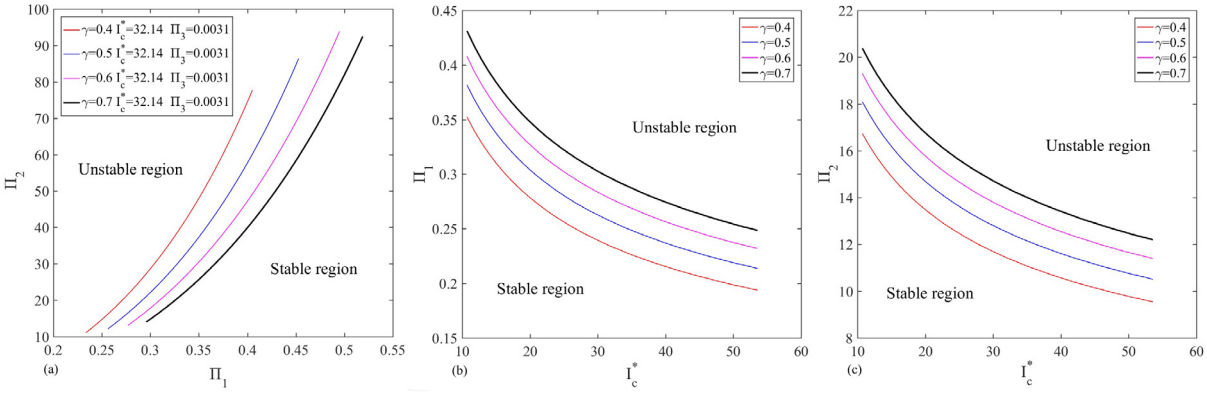

Fig. 9 Stability design charts as a function of Π_1, Π_2, γ and I_c^*. $I_a^* = 0.78$, $I_b^* = 0.03$ and $I_d^* = 0.19$.

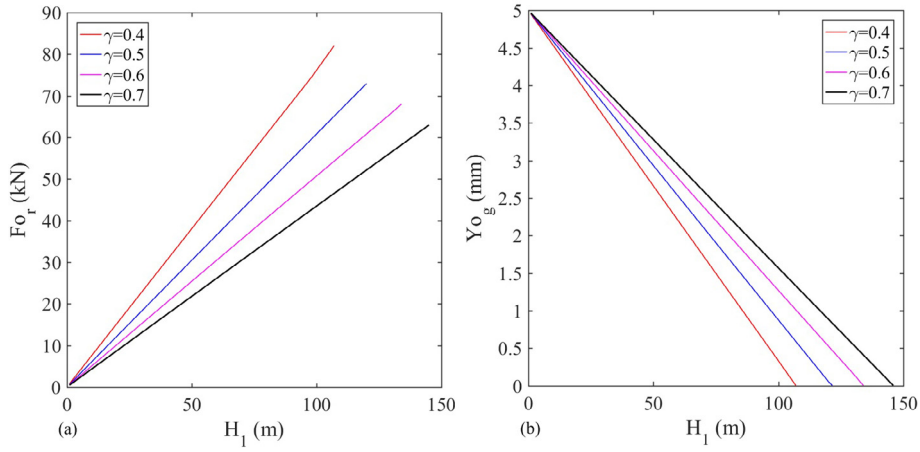

Fig. 10 Fo_r and Yo_g relation against H_1, keeping $I_a^* = 0.7811$, $I_b^* = 0.03$, $I_c^* = 32.14$ and $I_d^* = 0.19$.

Table 1 Relation between t_h and system pi groups keeping $I_a^* = 0.7811$, $I_b^* = 0.026$, $I_d^* = 0.1929$ as constants.

Π_1	Π_2	Π_3	γ	I_c^*	t_h
0.3651	17.2813	0.0031	0.4	32.144	1.018
0.5483	24.4397	0.0031	0.4	32.144	0.92
1.2612	42.3265	0.0031	0.4	32.144	0.819
0.3627	17.2813	0.0031	0.5	32.144	2.533
0.5405	24.4397	0.0031	0.5	32.144	1.05
1.1928	42.3279	0.0031	0.5	32.144	0.18
0.3609	17.2813	0.0031	0.6	32.144	3.005
0.5350	24.4397	0.0031	0.6	32.144	1.02
1.1475	42.3288	0.0031	0.6	32.144	0.91
0.5405	24.4397	0.0042	0.5	42.8587	0.923
0.5405	24.4397	0.0052	0.5	53.5733	0.923
0.5405	24.4397	0.0025	0.5	32.1440	0.926
0.5405	24.4397	0.0011	0.5	32.1440	0.925

Π_2. As seen, for the same γ and increasing I_c^* a lower Π_1 and Π_2 are needed to reach critical dynamic stability conditions. By increasing I_c^* the system tends to have a higher negative water damping such as mentioned in Fig. 8b. Also, for a higher γ values and varying I_c^* always a higher Π_1 and Π_2 are needed to overcome the added water damping to reach the critical dynamic stability condition.

Fig. 10 shows that increasing the input reservoir energy level the steady state hydraulic pressure force Fo_r tends to increase, which results in gap clearance reduction trying to achieve static stability condition. Also, by reducing γ static stability condition is achieved at a lower H_1, as increasing A_{os} results in Fo_r augmentation in a higher rate than structure stiffness augmentation leading to higher gap clearance closure.

After solving the system nonlinearly and including the neglected losses, the limit system oscillation amplitude cannot be obtained, as the gap clearance is very small. So, after a specific time the seal will hit the ball surface going backward and forward. Table 1, shows the effect of the dimensionless Pi-groups on the time t_h needed by the seal to hit the ball surface. As it can be seen, for the same values of γ and I_c^* as Π_1 and Π_2 increases the seal tends to hit the ball faster as the added water damping tends to excite the system rather than damping it and the seal tends to be more flexible as the negative water stiffness increases such as shown in Fig. 7 a and b and 5 a and b. Also, for $\gamma = 0.5$ with varying I_c^* the seal tends to hit the ball surface at the same time as the system tends to have a lower damping equivalent coefficient but with a higher equivalent stiffness coefficient. Finally, for I_c^*, γ equals to 0.5 and 32.14 and a varying $\Pi 3$, it can be seen that as Π_3 increases the time needed by the seal to hit the ball increases too as the equivalent damping coefficient increases.

7. Conclusions

1. The simplified presented hydro-mechanical model can predict the unstable and stable operation of each group of the Salime hydroelectric power plant taking into consideration varying system operation settings. Also, it is confirmed that the phenomenon is related to movement induced excitation flow induced vibration, as there is an unstable coupling between flow and seal vibration movement. The system may be initially under equilibrium but a small perturbation can lead to flow and pressure oscillations of incrementing or decaying amplitudes depending on stability conditions.
2. The added water mass is hardly influenced by the leakage flow. The added water mass is a function of pilot pipe line geometry and seal surface area ratio. Also, if the seal moves, the water at the pilot pipeline has to move along with the same velocity of the seal, as it is locked in sideways whatever the pilot line resistance is.
3. Static stability condition is not necessary to be achieved at very high input reservoir energy level as it depends on seal geometry affecting hydraulic pressure forces and seal structure stiffness. Although, adding an auxiliary system such as a compressor air system, which aims to augment pressure forces acting on the seal, will enhance system stability.
4. Seal dynamic instability is less prone to occur when operating at low gap kinetic energy to main line inertia ratio (Π_1) and gap reduced velocity (Π_2) (i.e. low input reservoir energy level), as the seal inlet velocity is higher than seal outlet velocity, which results in a positive water added damping. Besides, incrementing the external surface area of the seal to the seal surface area facing the gap flow (γ) improves system dynamic stability as the seal outlet velocity tends to decrease. Also, augmenting pilot pipe line resistance tends to improve added water damping and system dynamic stability.
5. Design stability charts demonstrated that for the same Π_2 a higher Π_1 is needed to reach critical stability conditions for a higher values of γ and same pilot pipeline water inertia coefficient to main line water inertia coefficient (I_c^*). However, for the same Π_1 a lower Π_2 is needed. Also, for the same value of γ and a varying I_c^* a higher Π_1 and Π_2 are needed for a lower I_c^* to reach critical stability condition.

Declaration of Competing Interest

The authors declared that there is no conflict of interest.

Acknowledgements

The authors acknowledge the financial support received from the Principado de Asturias (Spain) under grant FC-GRUPIN-IDI/2018/000205, as well as from the Arab Academy for Science, Technology & Maritime Transport (AASTMT) for PhD financial support and the Erasmus scholarship grant KA107 awarded to Mr. Hesham Awad. Special thanks are given to Mr. Alberto Rúa-Figueroa, manager of the Salime hydropower plant, for his collaboration and assessment.

Appendix A.

$$M_w^* = \left(\beta I_d^* \frac{\Pi_d}{1+4\Pi_1^2} - I_d^* \beta\gamma + I_p^*\right) \tag{A.1}$$

$$C_w^* = \frac{\frac{\Pi_d}{1+4\Pi_1^2}\left(2\beta\Pi_d w\left(1-I_d^*\right) - \frac{4\Pi_2\Pi_1^2\gamma w}{A^*}\right) + w\Pi_3}{W_{ref}} \tag{A.2}$$

$$K_w^* = \frac{\frac{\Pi_d}{1+4\Pi_1^2}\left(-4\beta\Pi_1^2 w^2 - \frac{2\Pi_2\Pi_1\gamma w^2}{A^*}\right)}{{w_{ref}}^2} \tag{A.3}$$

where

$$\beta = \frac{1-I_b^*}{1-I_d^*} - \gamma, \quad I_p^* = I_c^* + \frac{1}{\frac{1}{I_a^*}+\frac{1}{I_b^*}}, \quad \Pi_d = 1 - I_b^* - I_d^*(1-\gamma).$$

References

[1] E.B. Wylie, V.L. Streeter, Fluid Transients, McGraw-Hill, United States of America, 1978.

[2] M.H. Chaudhry, Applied Hydraulic Transients, Litton Educational, United States of America, 1979.

[3] https://www.saltosdelnavia.com/en/salime-hydropower-plant_57936.html.

[4] H.F. Abbott, W.L. Gibson, I.W. McCaig, Measurements of auto-oscillations in a hydroelectric supply tunnel and penstock system, Trans. Am. Soc. Mech. Engrs. 85 (1963) 625–630.

[5] E.B. Wylie, V.L. Streeter, Resonance in Bersimis no. 2 piping system, J. Basic Eng. 87 (1965) 925–931.

[6] J.H. Gummer, Penstock resonance at Maraetai 1 hydro station, Int. J. Hydropower Dams, UK (1995) 50–56.

[7] S.E. Kube, A.D. Henderson, J.E. Sargison, Modelling penstock pressure pulsations in hydro-electric power stations, 17th Australasian Fluid Mechanics Conference. Auckland, New Zealand, 2010.

[8] E. Naudascher, D. Rockwell, Flow-Induced Vibrations-an Engineering Guide, A.A. Balkema, Rotterdam, 1994.

[9] P.A. Kolkman, T.H.G. Jongeling, Dynamic Behaviour of Hydraulic Structures, Deltares, WL, 2007.

[10] D.S. Weaver, F.A. Adubi, N. Kouwen, Flow induced vibrations of a hydraulic valve and their elimination, J. Fluids Eng. 100 (1978) 239–245.

[11] D.S. Weaver, S. Ziada, A theoretical model for self-excited vibrations in hydraulic gates, valves and seals, J. Press. Vess. Technol. 102 (1980) 146–151.

[12] W.D. Netto, D.S. Weaver, Divergence and limit cycle oscillations in valve operating at small openings, J. Fluids Struct. 1 (1987) 3–18.

[13] S. Hayashi, Instability of poppet valve circuit, JSME Int. J. 38 (1995) 357–366.

[14] H. Ecker, A. Tondl, On the suppression of flow-generated self-excited vibrations of a valve, in: Vibration Problems ICOVP 2011, The 10th International Conference on Vibration Problems. Prague, Czech Republic, 2011, pp. 793-–799.

[15] P. Moussou, R.J. Gibert, G. Brasseur, Ch Teygeman, J. Ferrari, J.F. Rit, Instability of pressure relief valves in water pipes, J. Press. Vess. Technol. 132 (2010), 041308 (7 pages).

[16] C. Bazso, C.J. Hos, An experimental study on the stability of a direct spring loaded poppet relief valve, J. Fluids Struct. 42 (2013) 456–465.

[17] T.C. Allison, K. Brun, Testing and modeling of an acoustic instability in pilot operated pressure relief valves, J. Eng. Gas Turb. Power 138 (2016), 052401 (6 pages).

[18] S.E. Bouzidi, M. Hassan, S. Ziada, Experimental characterisation of the self-excited vibrations of spring-loaded valves, J. Fluids Struct. 76 (2018) 558–572.

[19] C. Hos, C. Bazso, A. Champneys, Model reduction of a direct spring-loaded pressure relief valve with upstream pipe, J. Appl. Math. 80 (2015) 1009–1024.

[20] A. Misra, K. Behdinan, W.L. Cleghorn, Self-excited vibration of a control valve due to fluid–structure interaction, J. Fluids Struct. 16 (2002) 649–665.

[21] R.G. Budyans, J.K. Nisbett, J.E. Shigley, Shigley's Mechanical Engineering Design, ninth ed., McGraw-Hill, New York, 2011.

[22] S.S. Raw, Mechanical Vibration, sixth ed., Pearson, 2017.

[23] J.M. Cimbala, Y.A. Cengel, Fluid Mechanics Fundamentals and Applications, second ed., McGraw-Hill, New York, 2009.